energies

MDPI

Article

Determination of the Required Power Response of Inverters to Provide Fast Frequency Support in Power Systems with Low Synchronous Inertia

Alejandro Rubio *, Holger Behrends, Stefan Geißendörfer, Karsten von Maydell and Carsten Agert

DLR Institute of Networked Energy Systems, Carl-von-Ossietzky-Str. 15, 26129 Oldenburg, Germany; holger.behrends@dlr.de (H.B.); stefan.geissendoerfer@dlr.de (S.G.); karsten.maydell@dlr.de (K.v.M.); carsten.agert@dlr.de (C.A.)

* Correspondence: alejandro.rubio@dlr.de; Tel.: +49-441-99906-481

Received: 29 December 2019; Accepted: 6 February 2020; Published: 13 February 2020

Abstract: The decommissioning of conventional power plants and the installation of inverter-based renewable energy technologies decrease the overall power system inertia, increasing the rate of change of frequency of a system (RoCoF). These expected high values of RoCoF shorten the time response needed before load shedding or generation curtailment takes place. In a future scenario where renewables are predominant in power systems, the ability of synchronous machines to meet such conditions is uncertain in terms of capacity and time response. The implementation of fast power reserve and synthetic inertia from inverter-based sources was assessed through the simulation of two scenarios with different grid sizes and primary reserve responses. As main results it was obtained that the full activation time for a fast power reserve with penetration above 80% of inverter-based generation would need to be 100 ms or less for imbalances up to 40%, regardless of the synchronous response and grid size, meaning that the current frequency measurement techniques and the time for fast power reserve deployment would not ensure system stability under high unbalanced conditions. At less-unbalanced conditions, the grid in the European scale was found to become critical with imbalances starting at 3% and a non-synchronous share of 60%.

Keywords: fast power reserve; frequency nadir; critical time; low inertia grids

1. Introduction

As part of the international efforts set to counteract global warming, the deployment of renewable energy sources in the electric sector has been considered an energetic priority as a measure to reduce CO_2 emissions. This objective is also reflected in the regulatory energy policies and plans of some countries. For instance, in Germany, the transformation of the electricity sector contemplates achieving a share of electricity generation of 80% from renewable energy by 2050. As part of such transformation, the expansion of renewables and the decommissioning of conventional power plants is regulated by the "Erneuerbare Energien Gesetz" [1]. The commitment of renewable energy plants has dispatch priority in the power market due to its zero marginal cost for power generation. This affects market auctions and also has some technical implications [2]. Balancing of the residual load is provided by conventional units, so curtailment of renewable energy resources is the least preferred option for power balancing [3].

An effect of conventional power plant decommissioning and their replacement with inverter-based renewable power plants is the reduction of system inertia, and consequently the incrementation of the rate of change of frequency (RoCoF) [4,5]. The relevance of the inherent synchronous generator inertia is to avoid rapid changes in frequency as load-generation imbalances take place; in this way, enough time is

given for the primary power reserve activation to recover the balanced, stable conditions [6]. In future power systems dominated by non-synchronous generation, it is expected that the inverters will be able to provide ancillary services such as frequency and voltage regulation [4,6]. Thus, the future inverters must be capable of replacing synchronous machines, operate in a decentralised mode, and provide inertial and damping responses [7].

Some ancillary services have been included in the inverter capabilities. The inverter-based generation has been employed to contribute to frequency and voltage regulation. Through the implementation of the virtual synchronous machine concept, inertial and damping capabilities can be added to the inverters [7,8]. This allows islanded operation as well as frequency control. Another common technique is the emulation of the power-frequency droop characteristic of the synchronous machine [5,9]. This method provides a primary reserve response but lacks an inertial response during transients. Moreover, ramping capabilities of PV plants' inverters were studied in [10] for power reserving. Similarly, highly PV penetrated grids and the inverters' requirements to meet local codes were evaluated in [11,12]. Additionally, modified control strategies in the power electronics allow the controller to extract part of the stored kinetic energy in the rotating masses of the wind turbines [9,13].

In continental Europe, the frequency range between 49.8 Hz and 50.2 should be maintained by reserves after a power imbalance. The primary reserve of the interconnected system can withstand a power imbalance of 3 GW with a system load of 150 GW [14]. The reference incident case scenario with a power loss of 3 GW has been found adequate even with a high penetration of renewables [3,14]. Nevertheless, there will be still many hours with a positive residual load. The decommissioning of conventional power plants diminishes their capacity to provide balancing power services. At low inertia conditions, the system balance must be complemented with a non-synchronous reserve. Additional to the uncertainty of conventional generation availability in the German power system, it is also not clear whether instantaneous reserve services from abroad will be available and whether transmission capacities will be enough [3].

The scope of this investigation is to determine the conditions which should be fulfilled by the fleet of inverters connected in a low inertia grid. The required triggering time and power response to avoid under-frequency load shedding (UFLS) are estimated. The over-frequency phenomenon is treated with the same approach as the under-frequency case. The effectiveness of synthetic inertia is also evaluated. In order to assess the influences of the grid size, synchronous response, and model simplifications, two grid cases are employed. The IEEE 9 bus benchmark grid model and an electric power system in the European scale are considered for said purpose; a methodology to determine the inverter requirements to offer frequency support is developed.

2. Methodology

2.1. Frequency Limits and Inertia Constants

When the global security of the system is endangered and under/above frequency is experienced, the load shedding is activated and the system enters an emergency state. If the frequency exceeds the range between 47.5 and 51.5 Hz, a system blackout can hardly be avoided [14]. Consequently, the system will reach the so-called blackout state and will have to be restored. Before the blackout, the system tries to recover the balance by rejecting a partial load starting at 49 Hz as frequency decreases. On the other hand, curtailment thresholds between 50.2 and 50.5 Hz have been studied by ENTSOE for over-frequency scenarios [14]. In this research, a deviation of ± 1 Hz is used as a threshold before load shedding and curtailment starts. In the case of under-frequency, power is injected in the system, whereas in the over-frequency case, power is extracted from the grid. Hence, to keep frequency within such threshold, the investigated critical time and power response corresponds to the maximum allowed time for fast power reserve activation in both over and under-frequency.

Two terms commonly found in the literature of power system stability will be used in this section:

- **Inertia constant (H)**: It has units of seconds (s) and it is the ratio of the stored kinetic energy in the rotating masses of the machine (E_k in MWs) and its nominal capacity (S_{nom} in MVA).
- **Acceleration time constant (T_a)**: It also has the units of seconds (s), but this is the ratio of double the kinetic energy (MWs) and the generator nominal power output (P_{nom} in MW). The acceleration time constant is a measure of the system's robustness against disturbances. It could be interpreted as the required time to remove the kinetic energy from the rotating masses at the rate of the supplied power load. Thus, the higher the time constant, the higher the available kinetic energy. As the share of synchronous generation decreases, this constant decreases proportionally.

With f as frequency, f_0 as nominal frequency and ΔP as power imbalance, the swing equation can be expressed as follows [15]:

$$\frac{df}{dt} = \frac{\Delta P * f_0}{2 * H * S_{nom}} = \frac{\Delta P * f_0}{T_a * P_{nom}} = \frac{\Delta P * f_0}{2 * E_k} \quad (1)$$

In this paper, the inertia constant H is used for the description of inertia in wind turbines and single synchronous machine representation, whereas the system acceleration constant T_a is used to express the whole system inertia related to the load in terms of real power.

2.2. Frequency Support from Inverter-Based Generation

In this section, the methodology and considerations for the implementation of inverter-based generation for frequency support are explained.

2.2.1. Synthetic Inertia

Synthetic inertia is one of the techniques that manufacturers and researchers are considering to tackle the low inertia problem in power systems [16,17]. Frequency support through synthetic inertia was considered with the following assumptions [9,18]:

1. The power output from synthetic inertia is limited to 10% of the wind turbine nominal power.
2. Due to mechanical and thermal stresses, the additional power can be delivered only for a maximum time of 10 s.
3. It is assumed that all wind turbines operate at a nominal power output. The value of 1.5 MW was selected for said purpose.
4. The maximum allowable amount of kinetic energy to be extracted from the turbines was limited to half of the kinetic energy while the turbine operates at a nominal speed [19].

A control system is needed so the stored energy in the rotating blades can be extracted from the wind turbine. Equation (2) is obtained from the expression of power as the derivative of the stored energy. The additional extracted power from the wind turbine through the implementation of Equation (2) accounts for the synthetic inertia contribution [19]. Figure 1 represents the implementation of Equation (2) in MATLAB-Simulink. In the figure, the insertion of a filter at the output of the multiplication block can be seen [17,18]. A constant block K_i adjusts the response in the model. Since Equation (2) is given per unit, the output is multiplied by a constant P_{wt} representing the turbine rated power.

$$P_{pu}(t) = 2 * H_{wt} * \omega_{pu}(t) * \frac{d\omega_{pu}(t)}{dt} \quad (2)$$

where H_{wt} is the turbine inertia constant and ω_{pu} the rotational speed per unit.

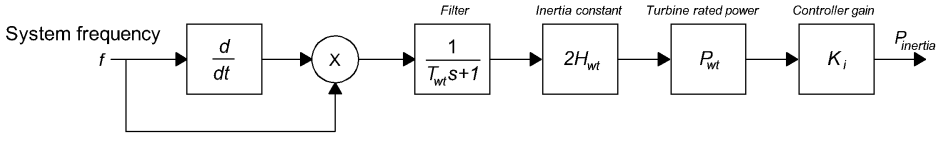

Figure 1. Block representation of Equation (2) in MATLAB-Simulink.

Typical values of inertia constant for wind turbines are not openly available from the manufacturers to the public. The approximate value was calculated with the utilisation of an equation which relates nominal power and inertia constant for wind turbines [20].

$$H_{wt} \approx 1.87 * P_{nwt}^{0.0597} \quad (3)$$

For a wind turbine with a nominal power of 1.5 MW, the value of H corresponds to 4.37 s. Rated rotational speed of 18 rev/min was considered [13]. To avoid the wind turbine stalling, a reduction of 5 revs/min is allowed. This change of rotational speed equals a reduction of 3 MWs on kinetic energy out of a total of 6 MWs. The values of the constants considered in the model are summarised in Table 1.

Table 1. Constants for the implementation of synthetic inertia. n_{wt} represents the number of wind turbines with synthetic inertia control.

T_{wt}	H_{wt} (s)	P_{wt} (MW)	K_i
1	4.37	1.5*n_{wt}	10

2.2.2. Inverter-Based Fast Power Reserve

When a power system is subjected to a negative power imbalance and it is assumed that no load is rejected at UFLS frequency, this continues dropping below 49 Hz. The time at which the system frequency equals the UFLS value is then called critical time. This is the maximum available time for the inverter-based reserve to deploy the required power to the system.

In the critical condition that would lead to load shedding, it is expected from the IBFPR to at least counteract the RoCoF at the critical time, as illustrated in Figure 2b. Recalling Equation (1); it is necessary that the machine accelerating power (power imbalance) becomes zero at the critical time.

$$P_a(t_{cr}) = P_{mech} - P_{elec} + P_{IBFPR} = 0 \quad (4)$$

where P_a is accelerating power, P_{mech} is mechanical power, P_{elec} is electrical power load, t_{cr} is the critical time, and P_{IBFPR} is inverter-based fast power reserve.

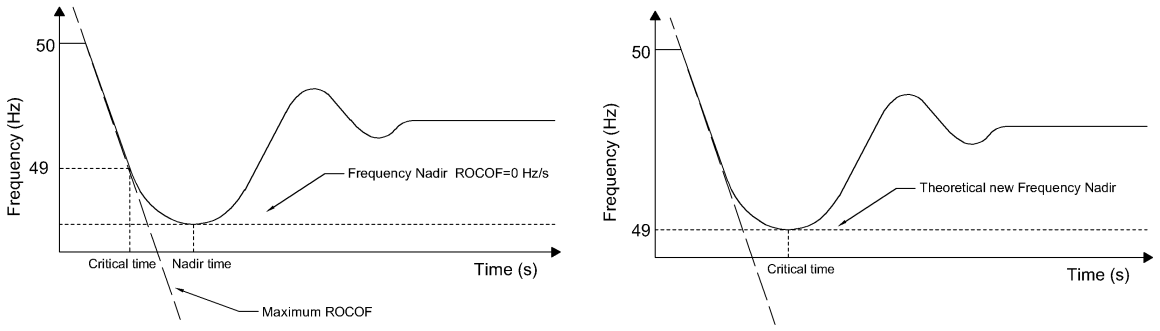

Figure 2. (**a**) Typical frequency response after a power imbalance leading to under-frequency load shedding (UFLS) at the critical time. (**b**) Power response with IBFPR applied to compensate power imbalance.

From the assumption of a linear mechanical power deployment of the synchronous machines governors, the rate of change in mechanical power, after a power imbalance ΔP, is given by $\Delta P / t_{nadir}$, where t_{nadir} represents the time at which the frequency nadir occurs. Given the power balance at the critical time, t_{cr}, the IBFPR response must be equal to $P_{elec} - P_{mech}$, P_{elec} being equal to ΔP.

Substituting P_{mech} by $\Delta P * t_{cr}/t_{nadir}$ and P_{elec} by ΔP in Equation (4), the following expression is obtained for the P_{IBFPR} at time t_{cr}:

$$P_{IBFPR}(t_{cr}) = \Delta P * (1 - t_{cr}/t_{nadir}) \tag{5}$$

It is assumed that P_{IBFPR} remains with a constant power output after t_{cr} long enough to stabilise the system frequency. The result of the previous equation represents the slope of the power output from the inception of the incident until the critical time, which with the implementation of IBFPR will not be critical any longer, but rather the new frequency nadir time.

$$P_{IBFPR}(t) = \frac{\Delta P * (1 - t_{cr}/t_{nadir}) * t}{t_{cr}} \tag{6}$$

According to the expression obtained in Equation (6), it can be realised that the desired power response from the inverters depends exclusively on parameters that cannot be directly measured from the grid. In a real situation, the values of ΔP, t_{nadir}, and t_{cr} cannot be known in advance; representing these factors is a challenge in the implementation of this ideal power response. Those values are dependent on the grid characteristics, the primary conventional reserve deployment time, and the overall system inertia [21]. Thus, two main cases are considered for the remaining analysis with the intent of covering a wider range of systems with different characteristics and dimensions.

2.3. Simulation Cases

As presented in the previous section, the values of critical time and frequency nadir depend on the system imbalance and primary reserve deployment time. In spite of assessing the influence of the grid size and the primary reserve characteristics, two main cases are considered. In Table 2, a summary of the simulated scenarios is provided. In both cases it is assumed that the initial steady frequency is the nominal 50 Hz.

- **Small scale grid case:** The IEEE 9 bus model was selected for carrying out the simulations due to its wide acceptance for power system studies and its relatively simple architecture [22,23]. The synchronous reserve deployment is in the order of a few seconds due to governor response [15,24]. In order to assess the typical simplifications made in power system analysis, two approaches of these cases were developed:
  - Scenario A—simplified model: The power system is represented by an equivalent single machine model in which the losses are neglected. In this case, typical governor data is considered [25]. With this model, the critical time and power response are determined. Furthermore, the impact of synthetic inertia is analysed.
  - Scenario B—extended model: All the power system components and their dynamic characteristics are considered in the IEEE 9 bus model for critical time and IBFPR estimation [22].
- **Large scale grid case:** The European grid-scale, in which all the synchronous machines are modelled and simplified as one single machine providing the characteristic expected from the overall system. The synchronous primary reserve deployment is in the order of $\approx$ 30 s [14,26]. The frequency response is assumed to be the same as the European response analysed by ENTSOE [14]. Similarly, as in the simplified model of the IEEE benchmark, the influence of synthetic inertia and IBFPR is evaluated.

Table 2. Summary of the simulated cases.

Cases	Assessment	
	IBFPR	**Synthetic Inertia**
Small scale grid		
(a) Simplified IEEE model	X	X
(b) Extended IEEE model	X	
Large scale grid	X	X

Therefore, with the selected cases, the critical and nadir times are estimated through the simulations of different scenarios combining a range of imbalances and shares of non-synchronous generation. In order to assess Equation (6), a fit of the critical time as function of RoCoF is carried out. With the corresponding fitting function for each case, Equation (6) can be easily applied assuming that the system inertia is known and power imbalance can be calculated as:

$$\Delta P(t) = \frac{df}{dt}\frac{T_a P_{LOAD}}{f_0} \tag{7}$$

2.4. Simplified IEEE 9 Bus Model

As a first step to evaluating the impacts of inverter-based generation and power imbalances in the grid, the whole system is simplified as one single generating unit. All the losses in the system (transformers, transmission lines, and generators) are neglected with the assumption that the prime mover output is the same as the electrical power output at the generator terminals. Table 3 provides a summary of the elements comprising the base model.

Table 3. Elements of the IEEE 9 bus model.

	Quantity
Buses	9
Transformers	3
Transmission Lines	6
Generators	3
Load	315 MW

Figure 3 is the block representation of the swing Equation (1); it only differs in the fact that additional blocks representing the inverter-based generation have been included. The mechanical power is represented by the output of a steam turbine governor model, which is used to represent the synchronous machine as depicted in Figure 4. In the figure, R is the turbine droop, P_{ref} is the reference load at nominal frequency, T_1 is the governor delay, T_2 is the reset time constant, T_3 is the servo time constant, T_4 is the steam valve time constant, and T_5 is the steam re-heat time constant [25]. When equilibrium is lost, the accelerating power is multiplied by the transfer function $1/(2HS)$, where H is the machine inertia constant and S is the machine power rating. From Equation (1) this product equals the derivative of frequency; therefore, an integrator block is added to obtain the frequency response [15,27,28]. A feedback loop is added and an error signal obtained from the reference frequency so that the synchronous machine can react as frequency deviates from the nominal value.

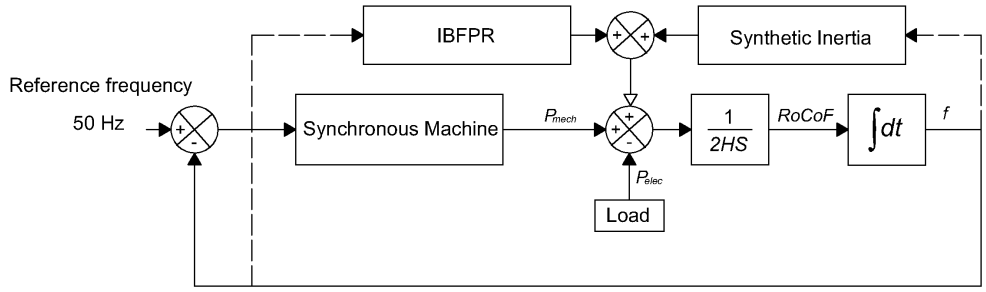

Figure 3. Simplified representation of the IEEE 9 bus model. Blocks linked by the solid line represent the conventional swing equation given by Equation (1). Represented with dashed lines, the respective frequency signals to the blocks of IBFPR and synthetic inertia, which add power to the system.

Typical governor constants are listed in Table 4. The values of kinetic energy and time constants of a synchronous machine with 835 MVA capacity were selected to represent the synchronous response; with a load of 315 MW, the system acceleration time constant is 14 s, which is approximately today's European acceleration constant [14]. This is the base scenario where a 100% synchronous generation is assumed. For the sake of evaluating the impact of the inverter-based generation penetration in the system, the values of lower capacity generators were selected, diminishing the total system inertia.

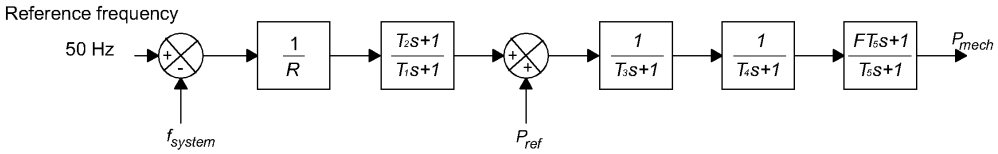

Figure 4. Model of the general-purpose governor for the representation of synchronous machines in the simplified IEEE 9 bus case.

Table 4. Typical generator values and governor settings as function of capacity [25]

Parameters	**Generator Capacity (MVA)**										
	911	835	590	410	384	192	100	75	51.2	35.29	25
T_1 (s)	0.1	0.18	0.08	0.18	0.22	0.083	0.09	0.09	0.2	0.2	0.2
T_2 (s)	0	0.03	0	0	0	0	0	0	0	0	0
T_3 (s)	0.2	0.2	0.15	0.04	0.2	0.2	0.2	0.2	0.3	0.3	0.3
T_4 (s)	0.1	0	0.05	0.25	0.25	0.05	0.3	0.3	0.09	0.2	0.09
T_5 (s)	8.72	8	10	8	8	8	0	0	0	0	0
Kinetic Energy (MWs)	2265	2206.4	1368	1518.7	1006.5	634	498.5	464	260	154.9	125.4
H (s)	2.486	2.642	2.319	3.704	2.621	3.302	4.985	6.187	5.078	4.389	5.016
P_{max} (MW)	820	766.29	553	367	360	175	105	75	53	36.1	22.5
T_a (s)	14.381	14.009	8.686	9.643	6.390	4.025	3.165	2.946	1.651	0.983	0.796

Even though load imbalances up to 40% were simulated in each inertia scenario, the capacity of the generator was disregarded for the estimation of the critical time. The negative imbalance was simulated by increasing the system load.

2.5. Extended IEEE 9 Bus Model

Since it was desired to compare the obtained results in Section 2.4 with some model that takes into account the whole system components, losses, and dynamics, an extended representation of the IEEE 9 bus model was implemented in MATLAB-Simulink [22]. In this representation, simulations for different values of system inertia and load imbalance were performed, similarly as was done with the simplified representation of the model. Figure 5 shows the extended IEEE 9 bus grid architecture with inverter-based generation added.

To evaluate the validity of the equation describing the IBFPR needed to avoid ULFS, the IEEE model was modified with the insertion of ideal controlled power source blocks. The power sources were set up to inject power into the grid according to the simulated scenario. Therefore, no means of frequency measurement were included, and only IBFPR was assessed. As it was done in Section 2.4, the total acceleration time constant of the system equalled 14 s for a complete synchronous generation share. Hence, the same kinetic energy should be distributed among the three rotating masses. From Equation (8), it can be easily calculated that the system's kinetic energy with 14 s of acceleration time constant is 2205 MWs.

$$T_{sys} = 2 * E_k / P_{load} \tag{8}$$

Since the inverter-based generation reduces the system's kinetic energy, for different levels of IBG, the generator nominal capacity was kept constant and the inertia constant of each machine multiplied by the synchronous share factor fss. The total system kinetic energy is the summation of all the machines kinetic energy.

To start the simulations in steady-state conditions, a load flow calculation of the grid was carried out to determine the initial conditions for the exciter and prime mover models. Table 5 summarises the main values for setting the system initial conditions from the load flow calculation.

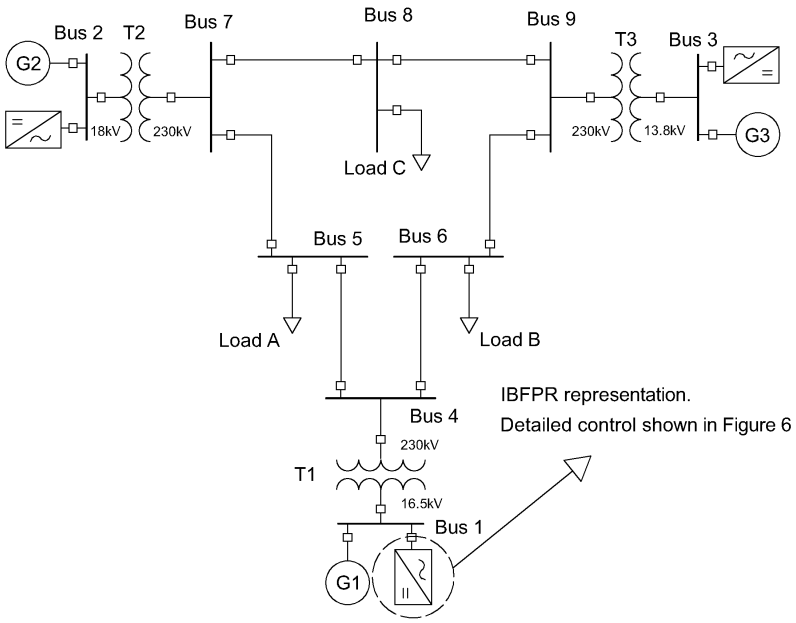

Figure 5. One line diagram of the IEEE 9 bus model. The inverter-based frequency response has been added at the same bus of the generating units.

Table 5. Steady state initial conditions of the system.

Bus Number	Bus Type	Voltage (pu)	Active Power (MW)	Reactive Power (MVAr)
1	Slack	$1.04\angle 0°$	72.2	25.64
2	PV	$1.025\angle 9.83°$	163	8
3	PV	$1.025\angle 4.63°$	85	−9.41
5	PQ	$0.9949\angle -4.42°$	125	50
6	PQ	$1.01211\angle -4.16°$	90	30
8	PQ	$1.0172\angle 0.17°$	100	35

IBFPR Representation

The IBFPR was modelled as controlled current sources. These controlled sources inject active power according to the load imbalance and system inertia simulated. The continuous measurement of voltage is required to determine the amount of current needed to supply the requested power. The IBFPR will have symmetrical and balanced characteristics. Due to that reason, the magnitude and angle of the current phasor will be obtained from the positive sequence of the measured voltage. From the definition of complex power and voltage symmetrical components in three-phase systems (9), the positive sequence components of the phase voltage and the line current are obtained [27].

$$S^1_{3\varphi} = 3 * V^1_{LN} * \bar{I}^1_L \tag{9}$$

This equation is valid for RMS values in which $S^1_{3\varphi}$ is the positive sequence of the three-phase complex power, V^1_{LN} is the positive sequence of voltage line to neutral, and $\bar{I}^1_L$ is the conjugation of the positive sequence line current. Nevertheless, the measured voltage values in MATLAB-Simulink are peak voltages, so the equations for power and current become:

$$S^1_{3\varphi} = \frac{3 * V^1_{LNpeak} * \bar{I}^1_{Lpeak}}{2} \tag{10}$$

$$I^1_{Lpeak} = \frac{2 * \bar{S}^1_{3\varphi}}{3 * V^1_{LNpeak}} \tag{11}$$

With the help of the **a** operator ($-0.5 + j\sqrt{3}$ or $1\underline{/120^\circ}$), the values of the positive sequence component of phase voltage can be obtained.

From $V_a + V_b + V_c = 0$ and $V^1_a = \frac{V_a + aV_b + a^2V_c}{3}$:

$$\begin{aligned} V^1_a &= \frac{V_a + aV_b - a^2V_b - a^2V_a}{3} \\ &= \frac{V_a * (1 - a^2) + aV_b * (1 - a)}{3} \end{aligned}$$

Since $V^1_{an} = \frac{V^1_a}{\sqrt{3}\underline{/30^\circ}}$, $\sqrt{3}\underline{/30^\circ} = 1 - a^2$ and $\sqrt{3}\underline{/-30^\circ} = 1 - a$ then after some algebraic manipulation, the expression for V^1_{an} becomes:

$$V^1_{an} = \frac{V_a - a^2V_b}{3} \tag{12}$$

With the obtained expressions in (12) and (10), the current needed (11) to supply the IBFPR related to the measured voltages can be implemented in MATLAB-Simulink, as depicted in Figure 6. From the voltages readings of lines a-b and b-c, the voltage V_{an} is calculated using Equation (12). Then, Equation (11) is implemented to calculate the current to be fed into the system using the complex power response (6) and the previously calculated value of V_{an}. The ramping function will last until the critical time is reached; afterwards, the IBFPR output will remain constant.

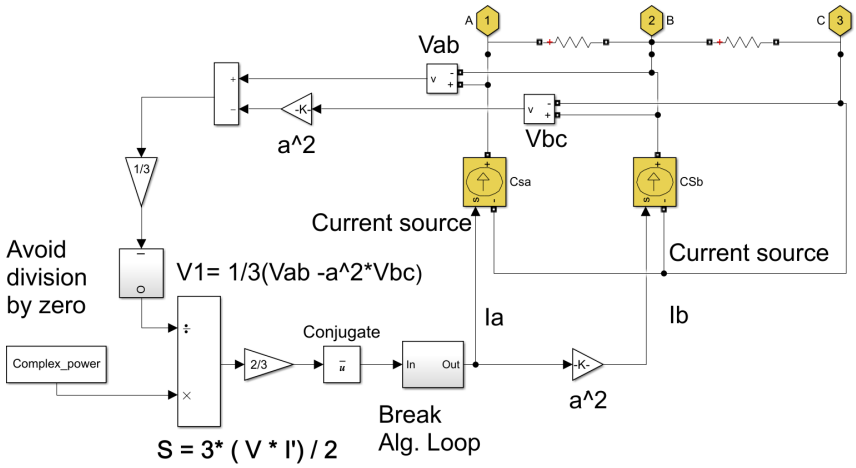

Figure 6. Implementation of IBFPR with ideal current sources and voltage monitoring in the extended IEEE model [29].

It must be noticed that when the IBFPR depicted in Figure 6 was implemented in MATLAB-Simulink, additional blocks were added to run the simulation; such blocks are a break in the algebraic loop just before the conjugate block. Additionally, a block to avoid division by zero was added at the output of the gain of 1/3 [29].

2.6. Large Scale Case: Europe Power System

Under normal operation, ENTSOE has reported values of RoCoF in the range of 5–10 mHz/s for power outages of 1 GW in the current interconnected power system. If an imbalance event of more than 3 GW occurs with depleted primary reserve, extraordinary values of frequency and RoCoF might be reached. After serious disturbances, the continental European power system has experienced RoCoF values between 100 mHz/s and 1 Hz/s. Imbalances of 20% or more along with RoCoFs greater than 1 Hz/s have been determined by experience to be critical [14]. ENTSOE has determined that in the interconnected reference scenario, the reduction of system inertia would not jeopardise the system's stability. Due to the expected increase of non-synchronous generation in the future, international power trade, and renewables' variability, ENTSOE estates in its future split reference scenario that the power system must be capable of withstanding imbalances greater than 40% with RoCoF values of 2 Hz/s or higher. Under these circumstances, the resulting islands must avoid load shedding. Hence, the conditions of the split scenario are considered for further analysis. The system representation is illustrated in Figure 7.

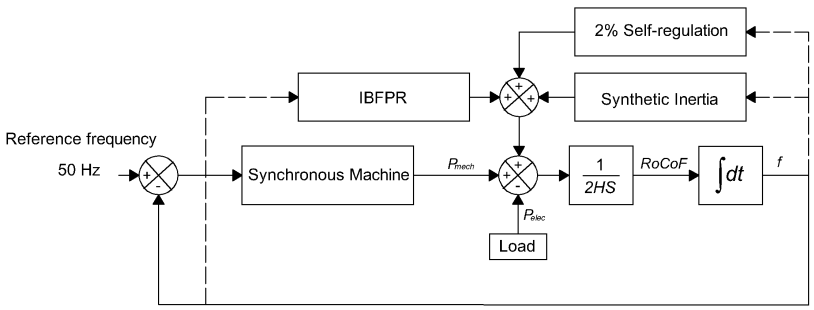

Figure 7. Large scale grid derived from the simplified IEEE model.

To fit the system behaviour to that modelled by ENTSOE, the synchronous representation in the simplified IEEE model shown in Figure 4 was used as a base. This was done with the insertion of an additional block at the output of the governor model, as shown in Figure 8. With this approach, the primary power reserve can be easily tuned with the assistance of the Control System Tuner

application available in MATLAB. In Figure 8, the synchronous machine block represents the governor model used in Section 2.4. The Control System Tuner sets the constants A, B, C, and D of the additional block in the model to have a step response with a rise time of ≈30 s by establishing an overshoot of 2% and a time constant of 8 s [28]. The time of utmost interest for analysis is from the inception of the power imbalance until the nadir time. Therefore, the system must perform as similarly as possible in this region compared to the ENTSOE reference, whereas after the nadir time, the disparity between responses can be neglected. On the European scale, the reserves must be completely deployed within 30 s after the occurrence of the disturbance.

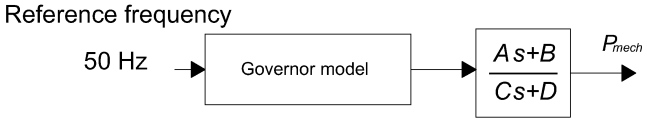

Figure 8. Governor representation for the large grid scale case.

System Parameters

When a power system with n number of synchronous machines is assumed, granting each of them a capacity of S MVA and a nominal power P_{nom} MW, and supposing that each machine operates at a deload factor dl of P_{nom}, with an acceleration constant equal to T_{nom}, then the number of machines n for the load $P_{syncload}$ served by synchronous machines is:

$$n = \frac{P_{syncload}}{P_{nom} * dl} \tag{13}$$

The system time acceleration constant T_{sys} can be obtained as follows:

$$\begin{aligned} T_{sys} &= \frac{\sum_{i=1}^{n} P_i * T_i}{P_{LOAD}} \\ &= \frac{nP_{nom} * T_i}{P_{LOAD}} \\ &= \frac{P_{syncload} * T_{nom}}{P_{LOAD} * dl} \\ &= \frac{Syncshare * T_{nom}}{dl} \end{aligned} \tag{14}$$

In this sense the system acceleration time constant can be calculated with a synchronous share of 100%, resulting in $T_{sys} = 12.5$ s with values of $T_{nom} = 10$ s [14,25], and a deload factor $dl = 0.8$. Considering only the swing equation, it can be demonstrated that RoCoF, and therefore, the frequency response of the system is only dependent on the percentage of load imbalance and the system acceleration time constant. From the definition of RoCoF as $\frac{df}{dt} = \frac{\Delta P * f_0}{2 * E_k}$ and $T_{sys} = \frac{2 * E_k}{P_{LOAD}}$:

$$\begin{aligned} \frac{df}{dt} &= \frac{\Delta P * f_0}{P_{LOAD} * T_{sys}} \\ &= \frac{\Delta P_{pu} * f_0}{P_{LOAD} * T_{sys}} \end{aligned} \tag{15}$$

In Equation (15) the value of ΔP_{pu} is the normalised value of power imbalance having as base power the value of load P_{LOAD}.

3. Results

3.1. Analysis of Critical Time

When the obtained critical times from the simplified and the extended model of the IEEE benchmark are compared in Figure 9, a higher deviation in the low range of RoCoF is clear. This is because the critical time is long enough to allow for the governor response activation of the respective synchronous machine's representation. Therefore, it can be stated that the simplifications made in the model have a greater influence on the results for low values of IBG penetration and low power imbalances. In this sense, the simplifications become less significant as the RoCoF increases in such a manner that the activated synchronous reserve is not relevant in frequency support. In the range of RoCoF higher than 2 Hz/s, the critical time trend for the European grid-scale and the simplified IEEE model get closer each to other as RoCoF increases.

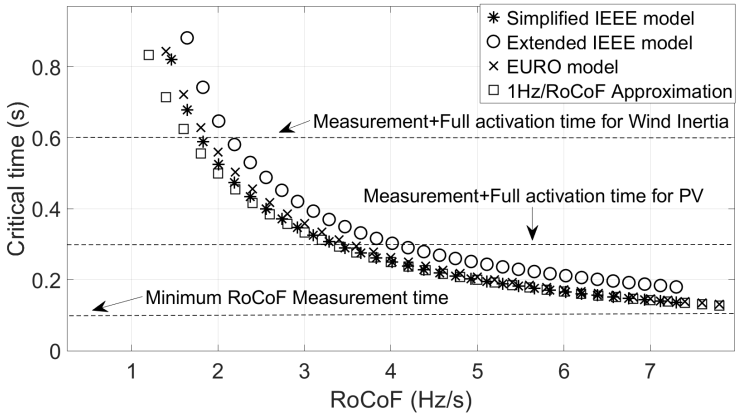

Figure 9. Results for critical time in all simulated models with a penetration of IBG of 80%.

Therefore under high RoCoF conditions in any of the models, the primary reserve does not significantly counteract the frequency drop [3]. Figure 9 demonstrates that primary reserve can be neglected for determining the critical time when the combination of IBG and load imbalances would lead to high RoCoF; as it increases, the approximation of critical time as 1 Hz/RoCoF narrows the difference with the results obtained from the simulations [30]. Nevertheless, such an approximation applies to the simplified IEEE model and the European-scale grid model. Hence, the influences of all the dynamics and machine components, such as the generator exciter and damping windings, seem to improve the critical time. The damping torque was not considered in Equation (1) for the simplified IEEE model; the inclusion of such may lead to more accurate results when compared with the extended model.

Because the European scenario's characteristics provided by ENTSOE were assumed to be the same as the resulting islands after a severe event; the results for the large scale model can be understood as the behaviour of the whole European system with bigger perturbations [14]. If in the future, a bigger reference scenario is utilised, then the synchronous response would not be enough to balance the system before load shedding occurs. Table 6 exhibits the required time when the power imbalance is increased by up to 10% for different IBG penetration.

Table 6. Critical time for European-scale case given in seconds.

IBG Share (%)	Load Imbalance (%)							
	3	**4**	**5**	**6**	**7**	**8**	**9**	**10**
20	-	-	6.081	4.517	3.629	3.050	2.638	2.316
40	-	6.226	4.169	3.215	2.628	2.222	1.934	1.705
60	7.142	3.639	2.623	2.062	1.698	1.451	1.263	1.122
80	2.753	1.744	1.277	1.018	0.843	0.722	0.628	0.559
95	0.697	0.436	0.322	0.254	0.211	0.179	0.157	0.140

3.2. *Analysis of Synthetic Inertia and Fast Power Reserve*

3.2.1. The Effect of Synthetic Inertia on Frequency

In this section, the results of the implementation of synthetic inertia in the simplified IEEE model and the European model are presented. The effect of synthetic inertia on the simplified model is illustrated in Figure 10a,b. Similarly, the effect of synthetic inertia on the European model is depicted in Figure 11a,b.

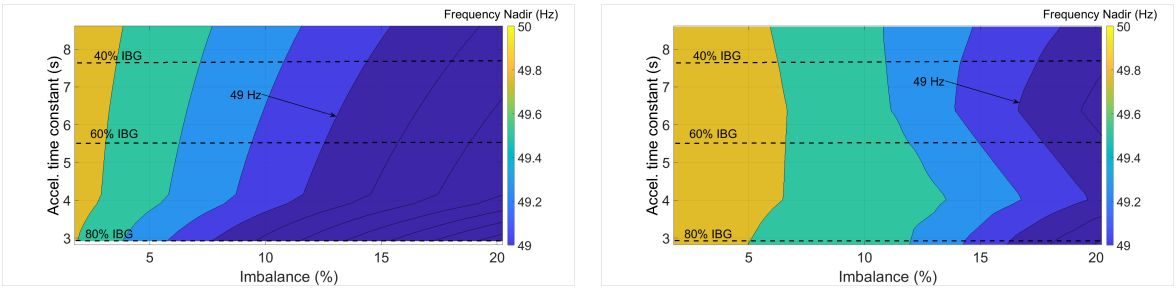

(**a**) (**b**)

Figure 10. (**a**) Frequency nadir of the simplified IEEE model with only synchronous reserve. (**b**) Frequency nadir of the simplified IEEE model with 40% of the IBG equipped with synthetic inertia controls.

In any of the cases, UFLS is not avoided for all combinations of imbalances and acceleration constants with the application of synthetic inertia. It can also be observed in Figure 10b that values of frequency nadir under 49 Hz are reached for imbalances bigger than 14% combined with IBG shares above 80% in the simplified representation of the IEEE model. Nevertheless, enhanced performance is observed in the simplified IEEE model. The reason behind this is the faster response of the synchronous share present in the system, which jointly performs with the synthetic inertia to improve overall frequency response performance. Conversely, the frequency nadir of the European-scale model, depicted in Figure 11b at 80% of IBG, reaches values lower than 49 Hz with an imbalance of 3%. This demonstrates that synthetic inertia is not enough by itself for withstanding severe imbalances under high penetration of inverter-based generation.

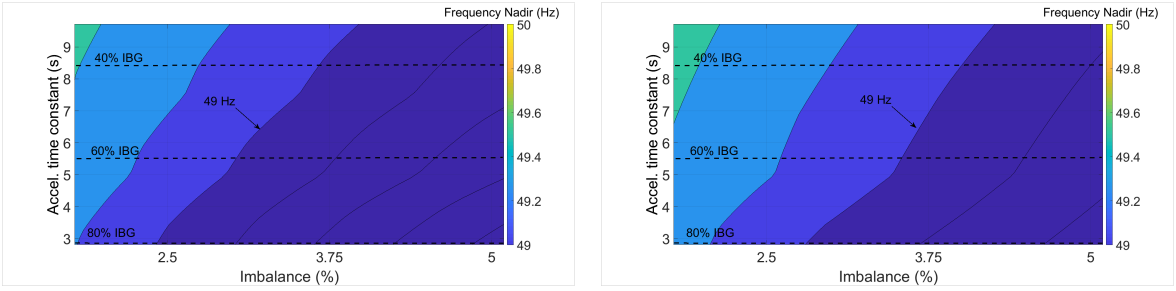

(**a**) (**b**)

Figure 11. (**a**) Frequency nadir of the European-scale with only synchronous reserve. (**b**) Frequency nadir of the European-scale model with 40% of the IBG equipped with synthetic inertia controls.

Figure 12a,b shows the frequency response of the system with wind shares of 40% and 80% out of the total IBG share. Power imbalances of 10% and 15% were considered for each. In Figure 12a it can be observed how the frequency drops below 49 Hz with a 10% of imbalance when no IBFPR or synthetic inertia is used as a frequency support strategy. There is an improvement of the response with the implementation of synthetic inertia. UFLS is avoided for every share of synthetic inertia, assuming that primary reserve takes place after synthetic inertia. As the imbalance increases, the effectiveness of the synthetic inertia decreases. Figure 12b shows how a wind power contribution of 40% from the inverter-based generation is capable of avoiding UFLS. Nevertheless, with the wind share of 80%, the frequency drops smoothly during a short period; then, suddenly, the frequency drops below 49 Hz, since synthetic inertia is switched off after 10 s. This situation leads to UFLS because frequency is sustained during that time by the synthetic inertia power.

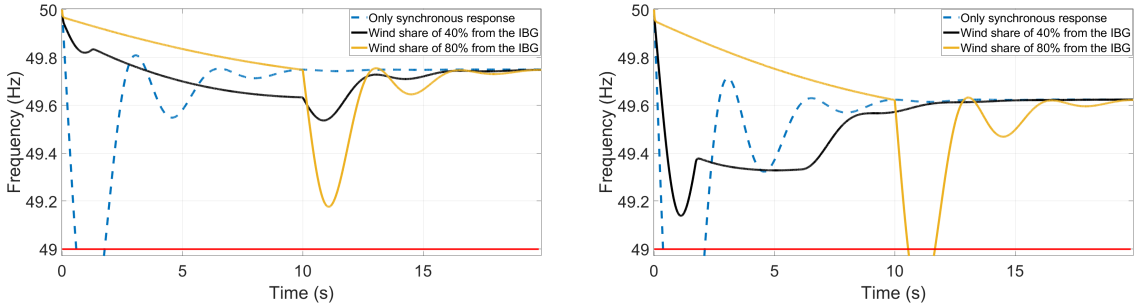

(**a**) (**b**)

Figure 12. (**a**) System frequency response and synthetic inertia performance with a power imbalance of 10%. (**b**) System frequency response and synthetic inertia performance with a power imbalance of 15%.

3.2.2. The Effect of Power Ramp Response on Frequency

The contribution from the ramping power in diminishing system RoCoF from the perturbation inception until the critical time was disregarded when the Equation (5) was calculated. Assuming an instant switch-on of the IBFPR at the critical time, the frequency nadir would be 49 Hz. However, a ramp power response was assumed instead. Therefore, the frequency response of an unbalanced system commonly exhibits a frequency nadir higher than 49 Hz due to the contribution of the ramping period. In this sense, it can be inferred that the longer the ramping period is, the higher the frequency nadir will be.

When a comparison is established between all the calculated power ramp slopes per unit (pu), with a high penetration of non-synchronous power in the system, the required power to ensure no UFLS has a consistent trend between the three models and proximity, is seen in Figure 13. A steeper power ramp slope is needed in all the range of RoCoF for the European case. After inspecting Equation (6), it was noticed that the IBFPR is affected by the factor $1 - t_{cr}/t_{nadir}$; then, as nadir time increases, IBFPR increases as well. The nadir time for the European case, due to the action of the self-regulation and primary reserve deployment of 30 s, is in the range of 3–12 s (6 s for 80% IBG penetration) whereas the nadir time for the simplified IEEE model is between 1 and 3 s.

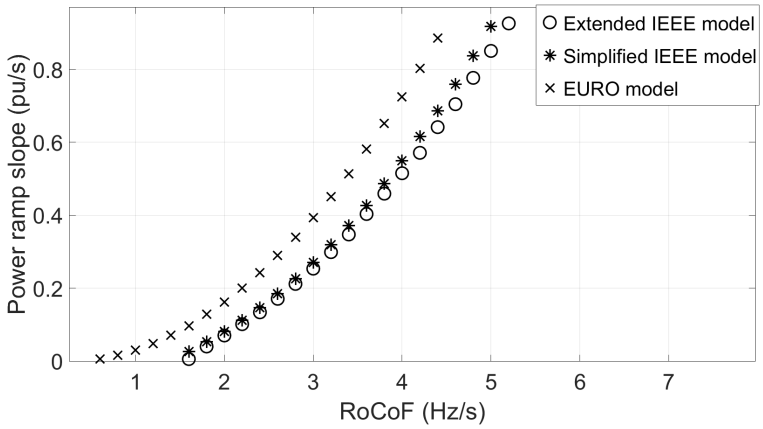

Figure 13. Comparison of the results of the three models in terms of the IBFPR power ramp which is needed at 80% of the share from non-synchronous generation.

3.2.3. Fast Power Reserve

The required power ramp to avoid load shedding has been found for both IEEE 9 bus models and the European-scale model. Hence, the IBFPR at the critical time, which remains constant after the critical time, would be counted as the fast power reserve. In Table 7 the required values for the inverter-based reserve for the European model are listed for imbalances out of the reference case of ENTSOE.

Table 7. Fast power reserve per unit for the European case with the power load as base.

IBG Share (%)	**Load Imbalance (%)**							
	3	**4**	**5**	**6**	**7**	**8**	**9**	**10**
20	-	-	0.025	0.038	0.049	0.060	0.070	0.081
40	-	0.016	0.030	0.041	0.052	0.063	0.073	0.083
60	0.005	0.024	0.035	0.045	0.056	0.066	0.077	0.087
80	0.016	0.028	0.039	0.049	0.062	0.070	0.080	0.09
95	0.024	0.035	0.045	0.055	0.065	0.075	0.085	0.096

When IBFPR is implemented in all three cases, the frequency drop below 49 Hz is avoided for almost all values of RoCoF, considering that enough IBFPR is available for the given imbalance. Figure 14a–c shows the frequency nadir for all the cases.

It can be observed that in the IEEE grid models, depicted in Figure 14a,b, UFLS is avoided in all the cases. However, in the simplified IEEE model, a minimum area with a value of 49.1 Hz is found, as indicated in the figure. This is caused because of the selected values of time constants for such inertia scenario. As indicated in Table 4, the generator with a capacity of 590 MVA has a bigger reheat time constant than the other machines, causing a delay in synchronous response. As the imbalance increases, the relevance of the response diminishes; therefore, the frequency nadir increases. In the case of the extended IEEE model, time constants were kept equal for all inertia scenarios, and only generator inertia was changed. In the European-scale model depicted in Figure 14c, UFLS is not avoided in the region of low imbalance and high acceleration time constant. Since the implemented IBFPR was based on a power response as a function of the measured initial RoCoF, the inaccuracy in the fitting function leads to overestimating the critical time in the low region of RoCoF as demonstrated in Figure 15. This has a bigger influence on the European-scale model because of the inaccuracy is not compensated by a faster power response from the synchronous machines.

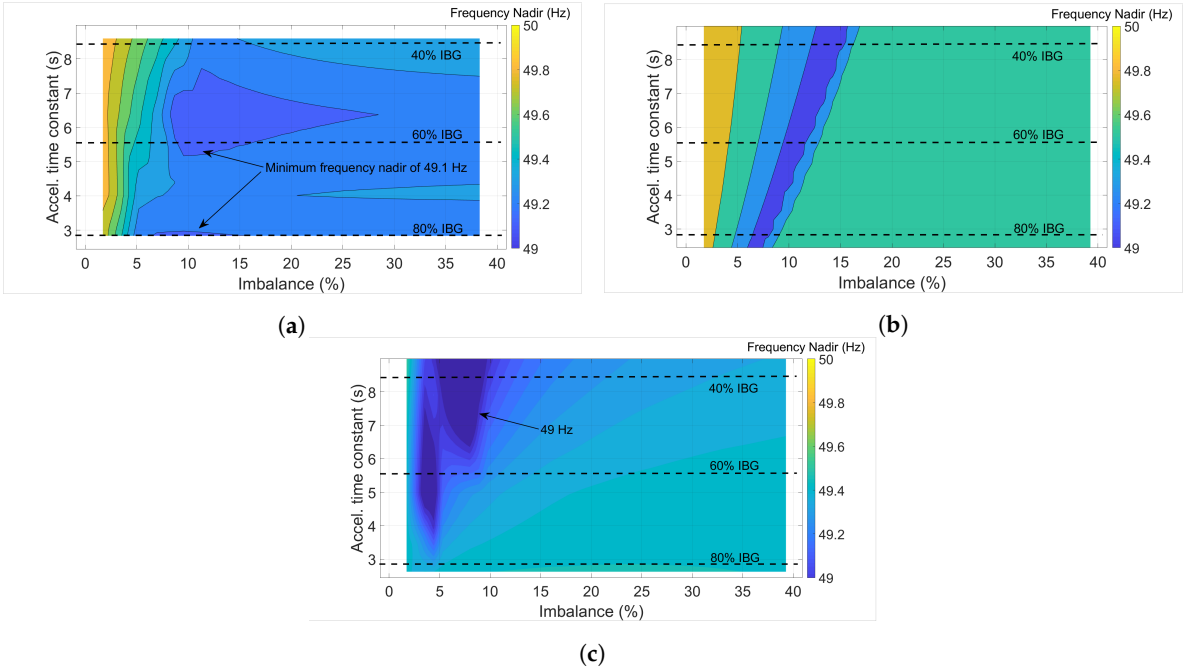

Figure 14. Frequency nadir with the implementation of IBFPR in: (**a**) The simplified IEEE model; (**b**) the extended IEEE model; (**c**) the large scale (European) model.

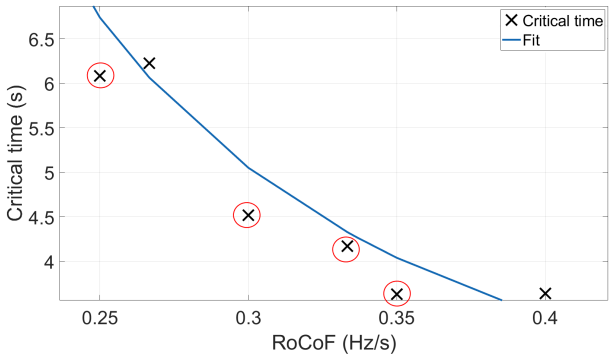

Figure 15. Overestimation of critical time leading to UFLS in the European-scale model.

3.3. Synchronising Effect, Lack of Damping Torque and Implications

The diminishing of synchronous machines in the system leads to a very weak network where synchronising and damping torque, which are inherent characteristics of synchronous machines, are not enough to stabilise the system [15]. Although the implementation of IBFPR contributes to keeping the synchronous machine on step, oscillations in the speed/frequency response of the rotor are observed. These oscillations are created by the lack of damping torque which is provided mainly by the synchronous machines through damping windings, a rotor field exciter, and a power system stabiliser [6,15].

For the simplified IEEE model and the European-scale model, only transfer functions describing an equivalent system governor were considered. Hence in such approaches, the effects and dynamics of a synchronous generator exciter and an inter-machine interaction were not taken into account. The aforementioned factors influence greatly the small-signal stability [15,25]. Even though the scope of this work was to analyse the power-time characteristics needed to avoid frequency collapse, oscillations were observed, but they could not be addressed by the simple injection of power to the system. With inverter-based generation penetration of 95%, and a 2% load imbalance being considered, UFLS is not reached, but the system becomes unstable, as shown in Figure 16a,b. With penetration levels above 85%, complete frequency stability is not ensured with the injection of a fast power reserve. Then, the system becomes unstable with increasing amplitude oscillations. It is important to note that ENTSOE in its EUROPEAN interconnected scenario determined that there is no UFLS when an imbalance of 2% with a high contribution of non-synchronous generation occurs. Nonetheless, no inter-machine interaction was considered, and therefore, a similar effect as observed in Figure 16a could be experienced.

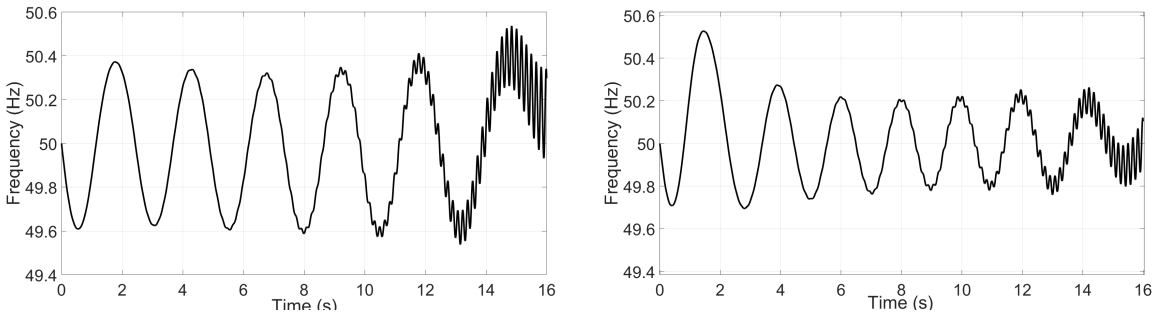

(**a**) (**b**)

Figure 16. (**a**) Oscillatory frequency response when no additional frequency support is given by the IBG. (**b**) Oscillatory frequency response when frequency support is given by the IBG.

Table 8 provides a summary of the main results obtained from the simulations.

Table 8. Summary of results.

	Main Results
European model	**1.** A load imbalance of 3% with an IBG share of 60% is critical. **2.** The power imbalances leading to UFLS must be covered almost completely by the IBFPR. **3.** The synthetic inertia does not substantially improve frequency nadir. **4.** The inaccuracy in the calculation of RoCoF leads to overestimation of the critical time, and consequently to UFLS.
Simplified IEEE model	**1.** The approximation of 1 Hz/RoCoF represents a good estimation of the critical time. **2.** An extreme power imbalance requires an activation time in the order of 100 ms. **3.** The frequency nadir was improved when synthetic inertia was implemented.
Extended IEEE model	**1.** The IBFPR does not provide damping torque to the system and undamped oscillations occur when the IBG share exceeds 85%. **2.** The critical time deviates from the simplified model the most when the RoCoF is low. **3.** A power rate in the range of 0.5 pu/s would be needed to avoid UFLS for conditions leading to RoCoF of 4 Hz/s. **4.** The faster synchronous response provides robustness when an inaccurate calculation of RoCoF is performed.

4. Discussion

The main results of the simulations are discussed in the following points:

- In the European scenario, the conventional governor response was found not to be able to ensure transient frequency stability in conditions of power imbalance exceeding 2%. A non-synchronous share of 60% with ≈ 3% power imbalance was found to be critical. The governor operation is too sluggish to constitute the unique solution for frequency support during the transient period. As indicated in [5], in real implementations, the governor response varies at each power plant, even having some of the governor response withdrawal. Thus, the inverter-based fast power reserve needs to be activated in an extremely short time.
- A fast power reserve activation between 0.14 and 2.75 s would be required for an inverter-based share above 80% and power imbalances between 3 and 10%.
- The uncertainty of synchronous reserve availability and possible power transmission congestion in future scenarios could lead to higher power imbalances, as occurs nowadays [3]. To avoid load shedding in scenarios with a non-synchronous share above 80% and load imbalances up to 40%, the inverter-based fast power reserve must be deployed in between 100 and 500 ms, independently of the grid size and the primary reserve response.
- Nevertheless, the currently full power activation time of renewable sources without storage is in the range of 200 to 600 ms. Table 9 lists some important and typical time scales of the most common power electronic technologies implemented in modern power systems. (Time required for the measurement, signal transmission, and processing, and the coordination of the power electronic controls [30].) These activation times are adequate for power imbalances leading to values of RoCoF equal or less than 4 Hz/s, as studied by ENTSOE for future scenarios [14].

Table 9. Activation time of non-synchronous technologies [30].

Technology	Full Fast Frequency Response (ms)
Wind turbine-Synthetic inertia	≈500
Lithium batteries	10–20
Flow batteries	10–20
Lead-acid batteries	40
Flywheels	<4
Super capacitor	10–20
Solar PV	100–200
HVDC	50–500

- The energy storage technologies will be a key factor to avoid deloading and curtailment of renewables. The fast activation time (<50 ms) and promising price reduction make storage a good strategy to provide power balancing in both over and under-frequency cases [31].
- With a non-synchronous share above 85%, the frequency excursions after a load imbalance do not exceed the stable threshold. Nonetheless, the total system stability is not ensured after a few seconds (≈5 s). The reduction of synchronous share provokes undamped oscillations due to the poor damping torque present in the system. Unlike the virtual synchronous machine [7], the proposed fast power reserve based on the initial RoCoF measurement does not provide damping torque, leading the system to become unstable for small perturbations [7,8].
- When a linear system is employed, as with the cases of the simplified IEEE model and the large scale scenario, no difference was found between the critical times for under and over-frequency. On the contrary, when the nonlinearity of the system is included in the extended model, the critical times between under and over-frequency do not match, as illustrated in Figure 17.

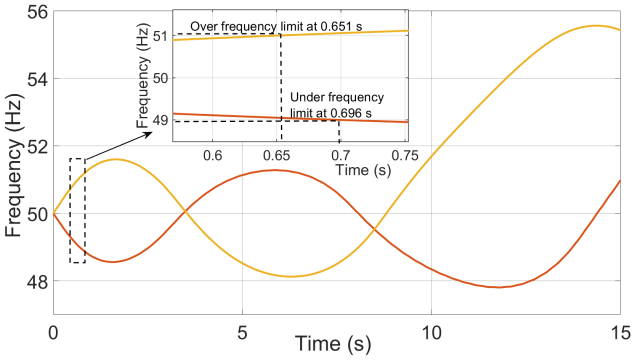

Figure 17. Under and over-frequency events in the extended IEEE model: a difference of 45 ms between each critical time was found.

- The synthetic inertia from wind turbines has a better performance when operated along with a fast synchronous response, as shown in Section 3.2.1. When synthetic inertia is implemented with a slow primary response, such as the case of the European grid, no frequency nadir improvement was obtained. Therefore, synthetic inertia is not able by itself to regulate or restore frequency deviation [13]. This outcome limits its usage just for slowing down the frequency drop after a load event. The influence of the gain K_i is fundamental, since the choice of a specific value can avoid load shedding just for a certain range of imbalances. For instance, in Section 3.2.1 it was demonstrated that the chosen value for K_i is adequate for imbalances of 10%, but as the imbalance increases to 15%, the initial dependency of system to sustain the imbalance from the synthetic inertia makes the frequency rapidly drop after 10 s, when the synthetic inertia has been removed.
- In general, similar behaviour is exhibited from the different models and approaches, even though they differ considerably in size and complexity. Hence, the simplified block representation of the power system seems to be a fair way to sketch overall system's trends and responses. The differences among governor time constants were found not to be relevant in frequency studies. The difference in critical time estimation between a full grid simulation and a simplified model was calculated to differ between 20% and 35%; such a difference could be crucial in fast power reserve studies, and therefore, should be considered when precise applications are implemented. A comprehensive method for estimation of the inverter-based fast power reserve and critical time were developed and proved through the simulation cases.

Author Contributions: Conceptualisation, A.R., H.B., and S.G.; investigation, A.R.; writing—original draft, A.R.; supervision, H.B., S.G., K.v.M., and C.A.; writing—review and editing, A.R., S.G., K.v.M., and C.A. All authors have read and agreed to the published version of the manuscript.

Funding: This research received no external funding.

Conflicts of Interest: The authors declare no conflict of interest.

Abbreviations

The following abbreviations are used in this manuscript:

ENTSOE	European Network of Transmission System Operators for Electricity.
HVDC	high voltage direct current.
IEEE	Institute of Electric and Electronic Engineers.
IBFPR	inverter-based fast power reserve.
IBG	inverter-based generation.
PV	photovoltaic.
RoCoF	Rate of Change of Frequency.
UFLS	under frequency load shedding.
WSCC	Western System Coordinated Council.

References

1. Energiewende: What do the New Laws Mean? Ten Questions and Answers about EEG 2017, the Electricity Market Act, and the Digitisation Act. Available online: https://www.agora-energiewende.de/fileadmin2/Projekte/2016/EEG-FAQ/Agora_FAQ-EEG_EN_WEB.pdf (accessed on 31 July 2019)
2. Energiewende, A. *Flexibility in Thermal Power Plants–With a Focus on Existing Coal-Fired Power Plants*; Agora Energiewende: Berlin, Germany, 2017.
3. Deutsche Energie-Agentur GmbH (dena)—German Energy. *dena Ancillary Services Study 2030: Security and Reliability of a Power Supply with a High Percentage of Renewable Energy*; Deutsche Energie-Agentur GmbH: Berlin, Germany, 2014.
4. Kroposki, B.; Johnson, B.; Zhang, Y.; Gevorgian, V.; Denholm, P.; Hodge, B.M.; Hannegan, B. Achieving a 100% renewable grid: Operating electric power systems with extremely high levels of variable renewable energy. *IEEE Power Energy Mag.* **2017**, *15*, 61–73. [CrossRef]
5. Miller, N.W.; Shao, M.; Venkataraman, S. California ISO (CAISO) frequency response study. *GE Energy* **2011**, *9*.
6. Lammert, G.; Yamashita, K.; Ospina, L.D.P.; Renner, H.; Villanueva, S.M.; Pourbeik, P.; Ciausiu, F.E.; Braun, M. Modelling and dynamic performance of inverter based generation in power system studies: an international questionnaire survey. *CIRED-Open Access Proc. J.* **2017**, *2017*, 1899–1902. [CrossRef]
7. D'Arco, S.; Suul, J.A.; Fosso, O.B. A Virtual Synchronous Machine implementation for distributed control of power converters in SmartGrids. *Electr. Power Syst. Res.* **2015**, *122*, 180–197. [CrossRef]
8. Vorwerk, J. Small-Signal Analysis of Power Systems with Low Rotational Inertia. Master's Thesis, Swiss Federal Institute of Technology (ETH), Zurich, Switzerland, 2018.
9. Dreidy, M.; Mokhlis, H.; Mekhilef, S. Inertia response and frequency control techniques for renewable energy sources: A review. *Renew. Sustain. Energy Rev.* **2017**, *69*, 144–155. [CrossRef]
10. Crăciun, B. Grid Support in Large scale PV Power Plants Using Active Power Reserves. Ph.D. Thesis, Aalborg University, Aalborg, Denmark, 2014.
11. Hoke, A.F. *Fast Grid Frequency Support from Distributed Inverter-Based Resources*; Technical Report; National Renewable Energy Lab. (NREL): Golden, CO, USA, 2018.
12. Hoke, A.; Elkhatib, M.; Nelson, A.; Johnson, J.; Tan, J.; Mahmud, R.; Gevorgian, V.; Neely, J.; Antonio, C.; Arakawa, D.; et al. *The Frequency-Watt Function: Simulation and Testing for the Hawaiian Electric Companies*; Technical Report; National Renewable Energy Lab. (NREL): Golden, CO, USA, 2017.
13. Wu, L.; Infield, D.G. Towards an Assessment of Power System Frequency Support from Wind Plant—Modeling Aggregate Inertial Response. *IEEE Trans. Power Syst.* **2013**, *28*, 2283–2291. [CrossRef]
14. ENTSOE. *Frequency Stability Evaluation Criteria for the Synchronous Zone of Continental Europe*; ENTSOE: Brussels, Belgium, 2016.
15. Kundur, P.; Balu, N.J.; Lauby, M.G. *Power System Stability and Control*; McGraw-Hill: New York, NY, USA, 1994; Volume 7.
16. Gevorgian, V.; Zhang, Y.N. *Wind Generation Participation in Power System Frequency Response*; Technical Report; National Renewable Energy Lab. (NREL): Golden, CO, USA, 2017.
17. First International Workshop on Grid Simulator Testing of Wind Turbine Drivetrains. Available online: https://www.nrel.gov/grid/assets/pdfs/turbine_sim_12_advanced_wind_plant_controls.pdf (accessed on 29 May 2019)
18. Nesje, B. The Need for Inertia in the Nordic Power System. Master's Thesis, NTNU, Trondheim, Norway, 2015.
19. Muljadi, E.; Gevorgian, V.; Singh, M.; Santoso, S. *Understanding Inertial and Frequency Response of Wind Power Plants*; University of Texas-Austin: Austin, TX, USA, 2012.
20. González Rodriguez, A.G.; González Rodriguez, A.; Burgos Payán, M. Estimating wind turbines mechanical constants. *Renew. Energy Power Qual. J.* **2007**, *1*, 697–704. [CrossRef]
21. Ørum, E.; Kuivaniemi, M.; Laasonen, M.; Bruseth, A.I.; Jansson, E.A.; Danell, A.; Elkington, K.; Modig, N. *Future System Inertia*; Tech. Rep.; ENTSOE: Brussels, Belgium, 2015.
22. Delavari, A.; Kamwa, I.; Brunelle, P. Simscape power systems benchmarks for education and research in power grid dynamics and control. In Proceedings of the 2018 IEEE Canadian Conference on Electrical & Computer Engineering (CCECE), Quebec City, QC, Canada, 13–16 May 2018; pp. 1–5.

23. Demetriou, P.; Asprou, M.; Quiros-Tortos, J.; Kyriakides, E. Dynamic IEEE test systems for transient analysis. *IEEE Syst. J.* **2015**, *11*, 2108–2117. [CrossRef]
24. Sundaram, D.; Bhuiyan, M. Comparing and Evaluating Frequency Response Characteristics of Conventional Power Plant with Wind Power Plant. Master's Thesis, Chalmers University of Technology, Göteborg, Sweden, 2008.
25. Anderson, P.M.; Fouad, A.A. *Power System Control and Stability*, 2nd ed.; Wiley: New York, NY, USA; Chichester, UK, 2002.
26. Hultholm, C.; Wägar, N. *Optimal Reserve Operation in Turkey–Frequency Control and Non-Spinning Reserves*; Power-Gen Europe: Milano, Italy, 2015.
27. Grainger, J.J.; Stevenson, W.D. *Power System Analysis*; McGraw-Hill: New York, NY, USA, 1994; Volume 67.
28. Ogata, K. *Ingenieria de Control Moderna (Spanish Edition)*; Prentice Hall: Upper Saddle River, NJ, USA, 1999.
29. Mathworks. Available online: https://www.mathworks.com/help/physmod/sps/examples/24-hour-simulation-of-a-vehicle-to-grid-v2g-system.html (accessed on 15 August 2019).
30. Miller, N.; Lew, D.; Piwko, R. *Technology Capabilities for Fast Frequency Response*; Tech. Rep.; GE Energy Consulting: Schenectady, NY, USA, 2017.
31. Ralon, P.; Taylor, M.; Ilas, A.; Diaz-Bone, H.; Kairies, K. *Electricity Storage and Renewables: Costs and Markets to 2030*; International Renewable Energy Agency: Abu Dhabi, UAE, 2017.